The Performance of Concrete in a Marine Environment

M.D.A. Thomas and E.G. Moffatt
University of New Brunswick, Department of Civil Engineering, Fredericton, NB, Canada

ABSTRACT

This paper presents a summary of data from wide range of concretes following periods of marine exposure ranging up to 25 years. Data are presented from more than 100 different concrete mixtures. The various types of concrete include fibre-reinforced concrete (FRC), ultra-high performance concrete (UHPC), concrete with a range of supplementary cementing materials (SCM such as fly ash, slag, and silica fume) and replacement levels (e.g. up to 58% fly ash and 80% slag), lightweight-aggregate concrete (LWAC) and concrete containing alkali-silica reactive aggregate. Testing included measuring chloride concentration profiles, electrochemical corrosion measurements (for steel-reinforced concrete), and various electrical and mechanical properties, in addition to the examination of the microstructure. The data invariably show the importance of the binder type in terms of resistance to chloride ingress and the protection conferred on embedded steel reinforcement, however, the overall performance of SCM concrete was equivocal as high replacement levels were observed to lead to increased surface deterioration (scaling) in some cases. The performance of UHPC was exemplary with little significant chloride penetration and no evidence of surface deterioration after up to 20 years exposure and an estimated 2,000+ freeze-thaw cycles. Expansion (and cracking) due to alkali-silica reaction was observed to be reduced by seawater exposure but, perhaps more significantly, render air-entrained concrete highly susceptible to freeze-thaw damage when the expansion exceeded a certain threshold value. The data are discussed in terms of code requirements and the need for appropriate performance testing. The importance of long-term monitoring of concrete on exposure sites is also discussed.

Keywords: chloride, corrosion, fly ash, marine, silica fume, slag

1.0 INTRODUCTION

Marine environments represent some of the most aggressive environments for concrete structures, as the conditions can promote a variety of deterioration processes (Fig. 1). These include corrosion of embedded steel reinforcement, freeze-thaw and salt scaling damage, abrasion (due to ice and suspended particulate matter), and chemical alteration sometimes leading to softening of the paste due to the action of Mg^{2+}, CO_3^{2-} and SO_4^{2-} ions present in the seawater (Santhanam and Otieno, 2016). It has also been reported (Nishibayasi *et al.* 1992) that seawater may exacerbate alkali-silica reaction (ASR) but to varying degrees depending on conditions. The severity of the exposure depends on, among other things, the composition of the seawater (e.g. salinity), climatic conditions (e.g. temperature and number of freeze-thaw cycles), the action of waves and ice, and the "marine zone" (e.g. immersion, tidal, splash or spray zone) to which the concrete is exposed. Despite the severity of the exposure, concrete has been and is extensively used in marine environments (Alexander and Nganda, 2016) and is generally durable provided it is properly designed, proportioned and constructed.
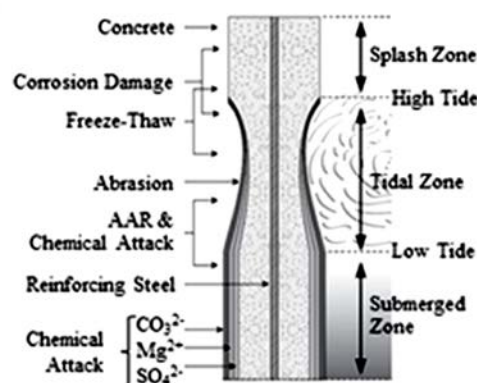
Fig. 1. Forms of attack in a marine environment (Modified from Mehta, 1980)

One of the more prevalent forms of deterioration for reinforced concrete in marine environments is the corrosion of embedded steel resulting from the penetration of chloride ions. Commonly-used measures to increase the resistance of concrete to the ingress of chlorides include reducing the water-to-cementing materials ratio (*w/cm*) and increasing the use of supplementary cementing materials (SCM) such as fly ash, silica fume, metakaolin and other pozzolans, and ground granulated blastfurnace slag.

Although the impact of SCM on chloride ingress in seawater has been recognized for many decades (Gjørv and Vennesland, 1979), there are still relatively few long-term data from SCM concrete exposed to seawater environments. Such information is vital to confirm the results from relatively short-term laboratory tests and for validating mathematical models for the predicting chloride ingress in concrete.

This paper presents data from two marine exposure sites, one on the Thames estuary in the U.K. and the other off the coast of Maine in the USA. A wide variety of concretes have been placed at these two sites on previous years and many of these have been retrieved and studied in the laboratory to determine the nature of the interaction between seawater and concrete, and the extent to which various materials can resist chloride penetration and corrosion. The data have also been used to validate a service-life model, Life-365, originally developed by the author and colleagues (Ehlen *et al.* 2009).

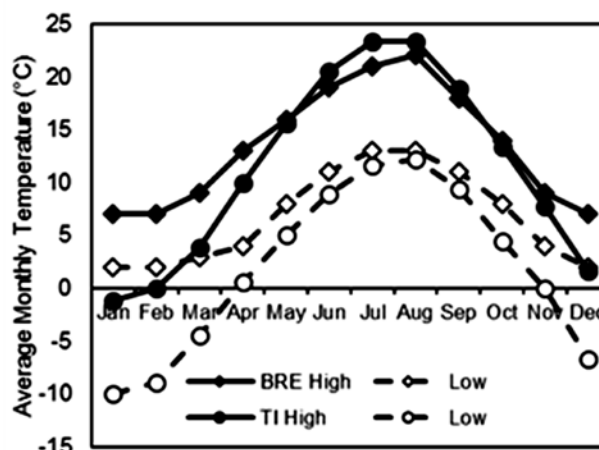## 2.0   MARINE EXPOSURE SITES

The Treat Island exposure site is in Passamaquoddy Bay just off the coast of Eastport, Maine, U.S.A. The site was developed by the U.S. Corps of Engineers in 1936. The BRE exposure site was located on the north shore of the Thames Estuary at Shoeburyness, Essex, U.K. Table 1 shows the composition of the seawater, tidal range and approximate number of freeze-thaw cycles per annum at each site. Figure 2 shows the average monthly high and low temperature for each site (note data are for Eastport, ME, and Southend-on-Sea for Treat Island and BRE, respectively). The exposure conditions at Treat Island are considered to be considerably more severe than those at BRE.

Table 1. Exposure conditions (g/L)

	BRE	Treat Is.
Composition of seawater (g/L)		
Cl	18.2	19.3
SO_4	2.6	2.7
Ca	0.4	0.4
Mg	1.2	1.3
Na	9.7	10.8
K	0.4	0.4
Total salinity	32.5	34.9
Tidal range (m)	5	6.7
Freeze-thaw (cycles/y)	100-160	20

The Treat Island site is still operational but the BRE site no longer exists. Both sites have or did have facilities to allow placement of specimens in the following exposure conditions: full immersion, tidal zone, or above high tide (splash zone). All of the data

presented in this paper relate to samples stored in the tidal zone of each site.

Fig. 2. Average monthly high and low temperatures for Treat Island (data for Eastport, ME) and BRE (data for Southend-on-Sea, EX) exposure sites

3.0   DETAILS OF CONCRETE MIXES AND TESTING

3.1   Test Program at BRE Exposure Site

The data presented in this paper for the BRE site were generated from 3 series of concrete mixes with strength grades of 25-MPa, 35-MPa and 45-MPa. Within each series concretes were cast with 0, 15, 30 or 50% fly ash (pulverized-fuel ash or PFA in the U.K.) produced from burning a bituminous coal. Concretes were designed for equal 28-day strength using the efficiency-factor concept such that within a given series the $w/(c+k \cdot f)$ was equal; where w = water, c = cement and f = fly ash contents (in kg/m^3) and k = efficiency factor for fly ash (= 0.3 in this study). Details of the materials used and the concrete mixture proportions are presented elsewhere (Thomas and Matthews, 2004).

Two types of specimen were placed at the BRE exposure site; these were: (i) 100-mm cubes – predominantly used for strength tests, but also used to determine wear ratings, and (ii) 100x100x300-mm concrete prisms, reinforced with four steel-bars, two with 10-mm and two with 20-mm cover – used to determine chloride profiles and gravimetric mass of steel bars.

Chloride profiles were determined by drilling concrete prisms with a rotary hammer drill (13-mm bit) in 5-mm increments, but discarding the outer 1-mm, and collecting the resulting dust samples. For each specimen tested at each age, eight samples (two per long face) were collected per sample and combined to produce dust samples with depth increments of 1-6 mm, 6-11 mm, … , 26-31 mm (or deeper in some cases). The dust samples were analyzed for total

chloride content and calcium (CaO) content by XRF and most of the data are presented as % chloride by mass of cementing material (cement + fly ash), the latter being calculated from the CaO content assuming the aggregate was free of calcium (Note: Thames Valley gravel and sand typically << 0.5% CaO).

3.2   Test Program at Treat Island

A wide range of concrete mixes cast using a variety of shapes and sizes have been placed at Treat Island since its construction in 1936. However, the data presented in this paper were collected from the following series of concretes:

- Concrete blocks placed by CANMET between 1978 and 1994; details of the 16 different phases of study including materials and proportions are provided in Malhotra and Bremner (1996). The testing was focused on the use of various SCMs with a range of replacement levels (up to 20% silica fume, 58% fly ash and 80% slag), including some ternary blends (Portland cement plus two SCMs). Other variables studied included the use of lightweight aggregate, steel fibres, plain and epoxy-coated steel, and reactive aggregates. In all but one case, the blocks produced measured 305x305x914-mm. The specimens containing reactive aggregate (Conrad greywacke from Nova Scotia) measured 381x381x711-mm. In nearly all cases, concrete mixes within a given mix series were cast with equal W/CM regardless of the SCM content. Between 2003 and 2018, as each concrete mixture reached an age of approximately 25 years, one block from each mixture was retrieved from Treat Island and taken to the University of New Brunswick (UNB) for testing.
- Blocks (900x900x900-mm) produced on-site during the construction of the Hibernia Gravity-Base Structure (GBS) using the production concrete; the blocks were shipped by barge and placed on the Treat Island exposure site in 1996. This concrete contained 470 kg/m³ of blended cement containing 8.5% silica fume, *w/cm* = 0.33, and the coarse aggregate was a 50/50 blend (by volume) of normal-density and lightweight aggregate (LWA).
- Concrete prisms from ultra-high-performance concrete (UHPC) mixes placed between 1995 and 2004. Three series of UHPC have been placed at Treat Island; these are: (i) very-high-strength concrete produced by the US Corps of Engineers (USCE) and placed in 1995 (designated VHSC), (ii) reactive-powder concrete produced by the USCE and placed in 1996 (designated as RPC 200), and (iii) reactive-powder concrete produced at UNB and placed in 2004 (designated UNB-RPC). Details of these mixes are presented by Thomas *et al.* (2012). All of the mixes met the general definition of UHPC being *composed of an optimized gradation of granular constituents, a water-to-cementitious*

materials ratio less than 0.25, and a high percentage of discontinuous internal fiber reinforcement, and compressive strengths of the mixes (with metallic fibres) prior to exposure at Treat Island was in the range of 155 to 215 MPa. All of the data presented in this paper were collected from concrete beams with dimensions 152x152x533-mm.

A wide range of tests have been performed at UNB on the blocks collected from Treat Island, but this paper focuses on the chloride profiles measured after 25 years' exposure to seawater, various mass transport properties determined on test specimens cut from the 25-year-old blocks and electrochemical corrosion tests (half-cell and linear-polarization resistance) performed on reinforced-concrete specimens

4.0   RESULTS AND DISCUSSION

4.1   Chemical Ingress/Attack

Figure 3 shows profiles for chloride, sulfate, water-soluble alkali, and magnesium determined on 30-MPa concrete prisms after 10 years' exposure on the BRE site. The chloride and sulfate contents were determined by XRF on fused beads produced from the dust samples. The alkali content was determined by flame photometry using a hot-water extraction technique. For each species the concentration, C_x, at depth, x, is normalized to the concentration, $C_{3.5}$, of the dust sample in the first depth increment (1-6 mm, average depth 3.5 mm).
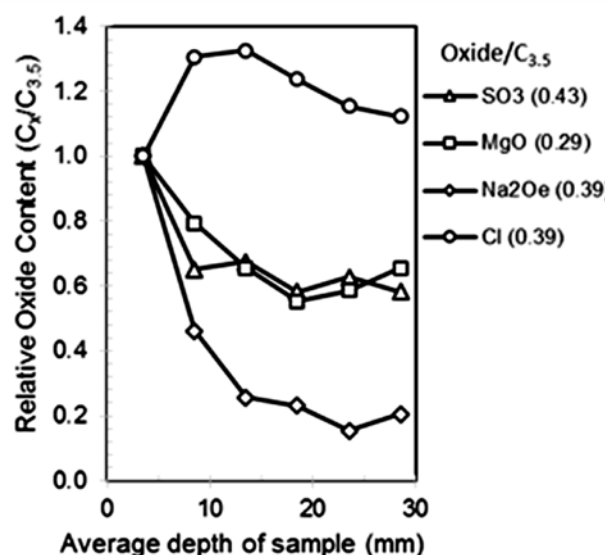

Fig. 3. Penetration of various species into 35-MPa Portland cement concrete after 10 years in the tidal zone at the BRE exposure site

The sulfate, magnesia and alkali contents showed similar trends with a significant increase in concentration in the 1-6 mm depth increment, a small

increase at 6-11 mm, and negligible augmentation below this depth. Contrarily, chloride penetrated to all depths measured and the concentrations (0.39 to 0.51% by mass of concrete) were high compared with background levels (< 0.02%) for the concrete. The low penetration of sulfate and magnesia may be partially explained by chemical binding as a result of reaction with the cement hydrates (see below). However, little binding of alkalis is expected with Portland cement. It is possible that some reaction of alkalis with the siliceous aggregate may have occurred but there was no evidence of this in microstructural examinations by scanning electron microscopy (SEM). The significant penetration of chloride ions without companion sodium ions from the seawater suggests that electro-neutrality is maintained by a counter-diffusion of hydroxyl ions [OH^-] from the concrete pore solution. This could explain the observation that exposure to seawater does not necessarily exacerbate alkali-silica reaction (ASR) in concrete containing reactive aggregate (see below).

Other workers have observed that Na and Cl do not penetrate at similar rates in Portland cement systems exposed to NaCl, with the penetration of Na being confined to relatively shallow depths (Johannesson *et al.*, 2007; De Weerdt *et al.* 2016).

Softening of the cement paste can occur in marine-exposed concrete primarily due to the interaction of the hydrates with Mg^{2+}, SO_4^{2-} and CO_3^{2-}, resulting in the formation of magnesium-silicate hydrates (M-S-H), thaumasite and aragonite among other phases. Brucite can also form in marine conditions but this tends to form a protective layer due to its low solubility rather than lead to softening. Figures 4 & 5 show, respectively, back-scattered electron (BSE) images and an X-ray diffractogram, showing the formation of these phases in the surface zone of the 25-MPa control (no SCM) concrete after 10 years in the tidal zone of the BRE exposure site.
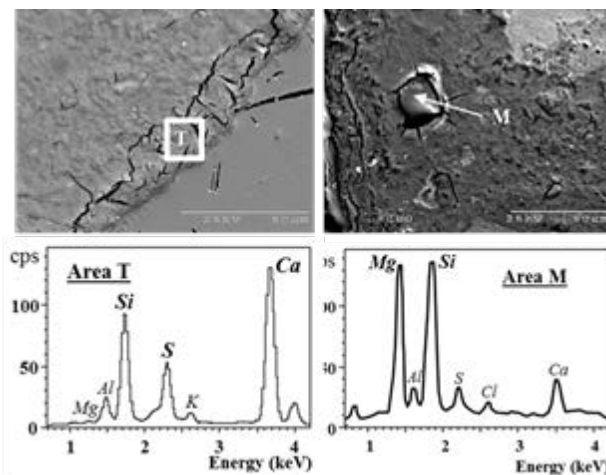
Fig. 4. BSE images showing thaumasite formation and M-S-H in 25-MPa concrete after 10 years exposure (BRE tidal)

These phases were relatively abundant but confined to the outer 1-6mm interval in the 25-MPa. The phases were generally less common in the higher grade concretes. This was consistent with the observations of wear (loss of edges and corners of cubes) and softening which were apparent on the 25-MPa concrete but absent on the 45-MPa concrete. It should also be noted that evidence of decalcification (lime leaching) of the surface layers was observed (not shown here), but the extent of the leaching also decreased with increased strength grade.
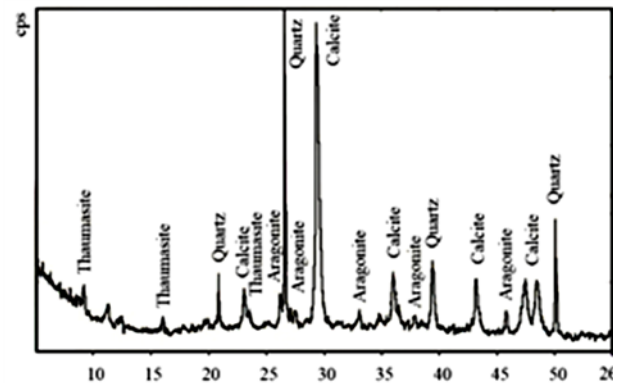
Fig. 5. X-ray diffraction pattern for 1-6mm dust sample from 25-MPa concrete after 10 years exposure (BRE tidal)

Softening and material loss of concrete is generally confined to the exposed surface zone of the concrete and occurs at an almost negligible rate in good quality (low-W/CM) concrete.

4.2   Seawater and Alkali-Silica Reaction

Figure 6 shows the expansion of concrete prisms (75x75x300-mm) containing a reactive flint sand in three different exposure conditions (all at 38°C) namely: (i) in sealed containers above water (e.g. 95% R.H.), (ii) in 5M NaCl, and (iii) in seawater collected from the BRE exposure site. Also shown is the expansion of large blocks (381x381x711-mm) containing reactive greywacke aggregate; one block from each of four mixes is stored outdoors on an exposure site near Ottawa, Canada, and a second block from companion mixes is in the tidal zone at Treat Island. The four mixes are: (i) high-alkali cement (HA), (ii) low-alkali cement (LA), (iii) HA with 20% fly ash, and (iv) HA with 30% fly ash. Details of the mixes and the exposure site in Ottawa can be found in Fournier *et al.* (2016).

Small concrete prisms (minimum dimension 75 mm) stored in seawater at 38°C did not expand in laboratory conditions whereas significant expansion occurred with companion prisms from the same mix either stored above water or in concentrated (5 Molar) NaCl solution. It is probable that hydroxyl ions (OH^-) were leached rapidly from the prisms stored in seawater, electro-neutrality being maintained by the combination of leaching of sodium (Na^+) and

potassium (K$^+$) ions and counter-diffusion of chloride ions (Cl$^-$).

Concrete blocks (minimum dimension 381 mm) did expand when exposed to tidal conditions at Treat Island but the expansion was lower than that of blocks with the same composition stored on an exposure site in Ottawa. The decreased expansion may be partly ascribed to the lower average temperature of the blocks at Treat Island which are immersed in cold seawater twice daily. However, it is noteworthy that the exposure to the external supply of sodium did not exacerbate ASR expansion.
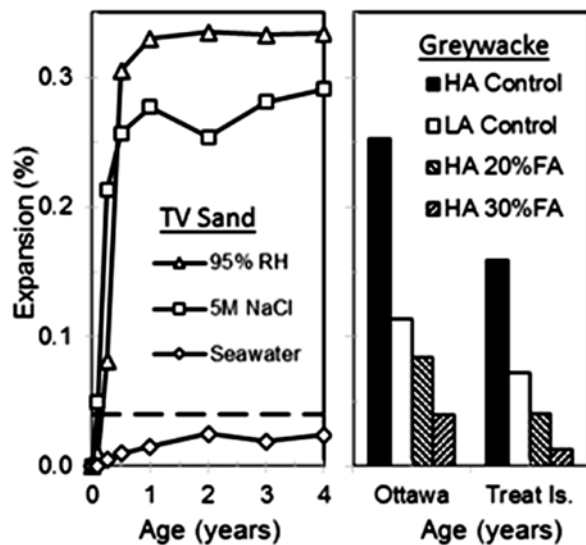
Fig. 6. Effect of seawater on expansion of prisms in the lab (left) and 13-year expansion of large blocks on outdoor and marine exposure sites (right)

Published data on the effects of NaCl exposure on ASR are equivocal; but the following summary observations have been made by Folliard *et al.* (2008) from a synthesis of the literature:

- High concentrations of NaCl (>> seawater) may exacerbate expansion in small samples containing certain types of highly reactive (opaline) silica,
- ASR may be decreased in thin elements exposed to seawater because of a decrease in pH,
- ASR is unlikely to be significantly modified in large elements because of the limited penetration of sodium.

The results of the testing presented here are generally consistent with these observations. This may be relevant to certain existing practices for minimizing the risk of ASR such as ASTM C 1778-16 *Standard Guide for Reducing the Risk of Deleterious Alkali-Aggregate Reaction in Concrete* which considers seawater exposure to present a higher risk of ASR than immersion in (plain) water and, consequently, requires a higher level of prevention to be applied in such cases. The data presented here would suggest that seawater is not a more aggressive

exposure in terms of ASR and that additional prevention is not warranted in marine environments.

4.3 Chloride Penetration

BRE Exposure Site
Chloride profiles were determined after exposure periods of 1 day, 28 days, 1, 2, 4 and 10 years and selected data have been reported previously (Thomas, 1991; Thomas and Matthews, 1996; 2004). The early-age data (1 and 28 days) were collected to determine the impact of initial absorption of seawater because the concrete samples were placed in an unsaturated condition (i.e. moist-cured for 1, 3 or 7 days followed storage in laboratory air until initial exposure at 28 days). Profiles for the 25-MPa and 45-MPa concretes after 10 years are shown in Fig. 7.
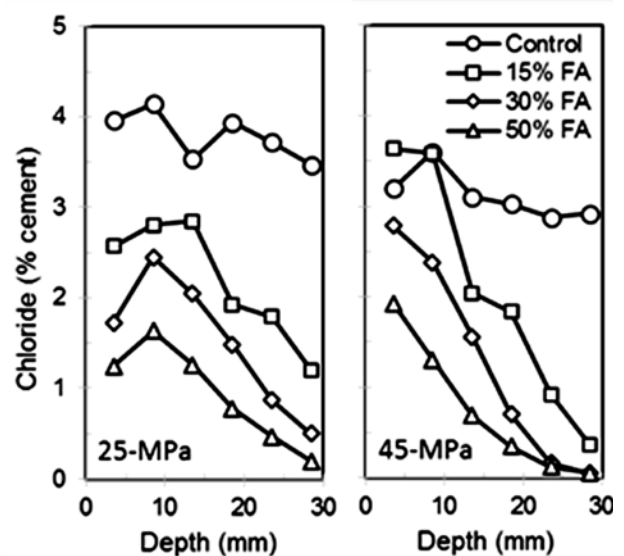

Fig. 7. Chloride profiles for 25-MPa (left) and 45-MPa concretes after 10 years in BRE tidal zone

The chloride profiles (Fig. 7) clearly show the very profound effect that fly ash has on the chloride ingress. Indeed incorporating 15% or more fly ash is considerably more effective than reducing the W/CM as can be seen by comparing the profiles for the 15-MPa and 45-MPa control concretes which have, respectively, W/CM values of 0.68 and 0.49.

Figure 8 shows chloride profiles after different periods of exposure (from 1 day to 10 years) for the 35-MPa concretes without and with 30% fly ash. After early periods of immersion (1d to 1y), the depth of penetration seems little influenced by the introduction of fly ash. However, the impact of fly ash in terms of reducing chloride penetration becomes evident after 2 years and is extremely pronounced at later ages (4 and 10y). The small differences in the early-age profiles may be partly due to the dominant effects of capillary suction on the concrete shortly after the seawater exposure of the unsaturated concrete. However, the growing influence of the fly ash on chloride penetration with age is undoubtedly due to the long-term reductions in the chloride transport

properties (e,g. diffusion) that have been attributed to fly ash and other SCMs (e.g. Thomas and Bamforth, 1999). This "age-effect" is further demonstrated in Fig. 9 which shows two parameters both plotted as a function of the square-root of the exposure period. The first parameter is the chloride content determined in the dust sample representing the 21-26mm depth increment. This is the deepest increment that was available at all exposure periods. The second parameter is the depth of penetration, x_{ct}, of the chloride threshold value, C_t. In this analysis a single value of $C_t = 0.4\%$ (by mass of cementitious material) is used for all concrete regardless of fly ash content; this value is a commonly-used chloride threshold in the literature (Angst *et al.* 2009).
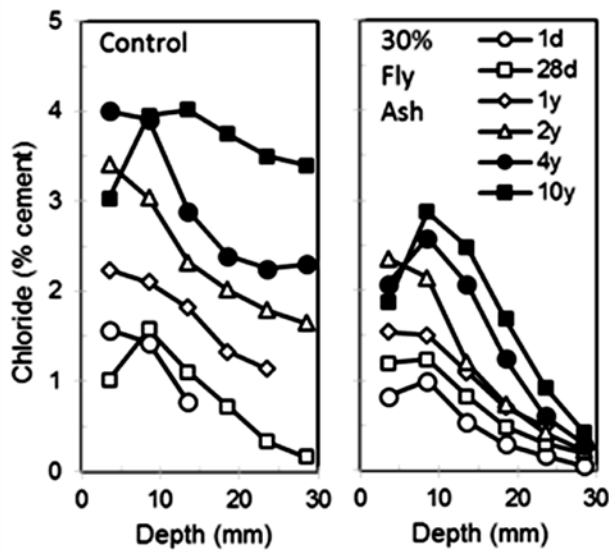
Fig. 8. Chloride profiles after various exposure periods for 35-MPa concretes without (left) and with (right) 30% fly ash.
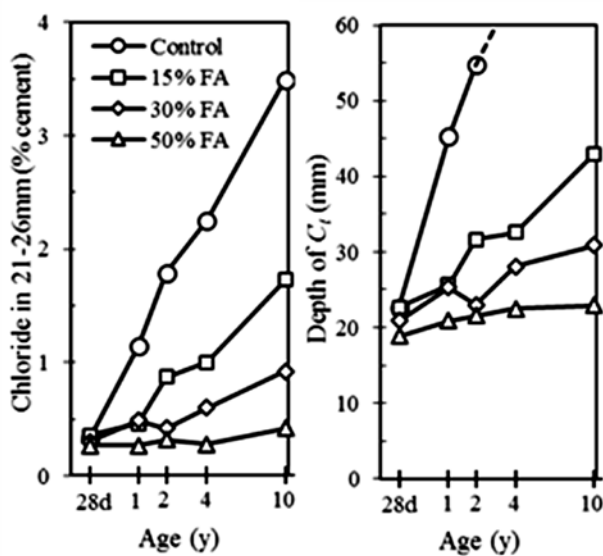
Fig. 9. Change in chloride content in the 21-26mm depth increment (left) and rate of penetration of C_t as a function of exposure period

The data in Fig. 9 clearly demonstrate that the increases in chloride resistance attributed to the use of fly ash intensifies as the concrete matures throughout the ten-year exposure period examined in this study. Despite the initially rapid penetration of chlorides to depths of approximately 25-mm or so in all of the concretes there is a very clear distinction with regards to longer-term penetration. For concrete with 30% or, especially, 50% fly ash the penetration of chlorides becomes very slow or virtually ceases beyond 4 years or so.

Treat Island Site: Effect of SCM's
Figure 10 shows chloride profiles for 17 different concrete mixes (5 controls plus 12 with varying levels of SCM) tested after 25 years in the tidal zone at Treat Island. SCM replacement levels included:
- 25 to 80% slag
- 25% low-calcium 'F' fly ash (note data for high-volume fly ash presented below)
- 20/40 and 20/60 fly ash/slag combinations
- 6.5/13.5 silica fume/fly ash combinations

Although a range of W/CM (up to 0.60) were used, the data in the figure are restricted to concretes with W/CM = 0.40 as this is generally considered to be the maximum recommended for reinforced concrete subjected to seawater.
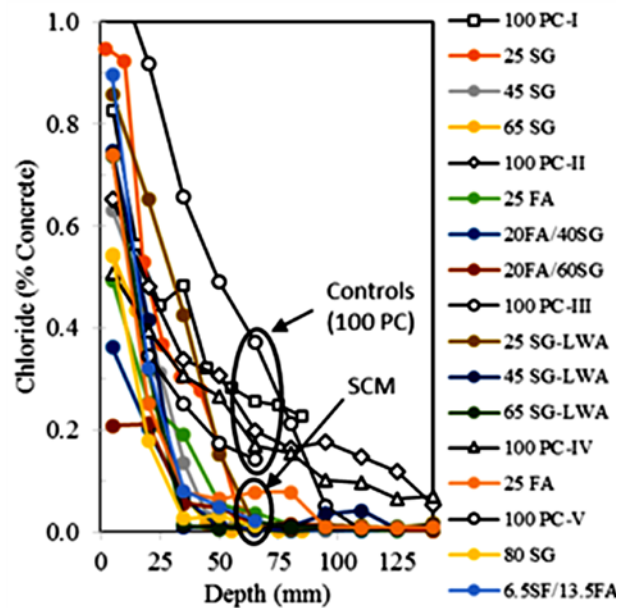
Fig. 10. Chloride profiles for concrete (W/CM = 0.40) after 25 years in the tidal zone at Treat Island

The five control mixes had the same W/CM (0.40) but the cementitious material content varied from 396 to 473 kg/m³. The control mix 100 PC-III had the highest cement content and also incorporated expanded shale lightweight aggregate (LWA) in the coarse fraction. This explains why the chloride concentration was increased close to the surface of this mix compared to the other controls.

The effect of SCM can be clearly seen in Fig. 10 as the chloride concentration decreases with depth more

6

rapidly with SCM concrete compared with PC concrete. In all cases the chloride content for the SCM concretes decreased to below 0.10% and, in all but one case (one of the two concretes with 25% fly ash), below 0.05%, in the sample representing the depth increment 60-70mm. The chloride content at the same depth ranged from 0.14 to 0.26% with an average value of 0.23% (or 0.19% if the concrete with LWA is excluded. Generally the concretes with the highest level of SCM (e.g. 65 and 80% slag, or a combination of 20% fly ash with 60% slag) had the lowest depth of chloride penetration.

Treat Island Site: High-Volume Fly Ash (HVFA)
Three series of HVFA concrete were placed at Treat Island; these were:
- Phase VIII (placed in 1987): 56% fly ash, w/cm = 0.31 to 0.35, normal density aggregates.
- Phase XI (placed in 1990): 56% fly ash, w/cm = 0.38, LWA coarse (three types).
- Phase XIII (placed in 1992): 58% fly ash, w/cm = 0.33, normal density aggregates.

Blocks were retrieved from selected mixes in 2011 when the concretes in Phases VIII, XI and XIII were, respectively, 24, 21 and 19 years old. Chloride profiles are presented in Fig. 11 for eleven HVFA mixes together with two control mixes (no fly ash) from Phase VIII with w/cm = 0.38 and 0.46. Full details of the mixes and testing can be found in Moffatt et al. (2017).
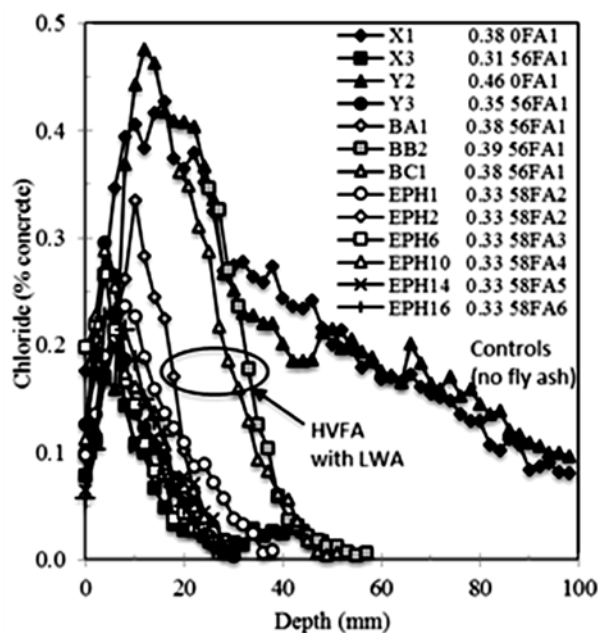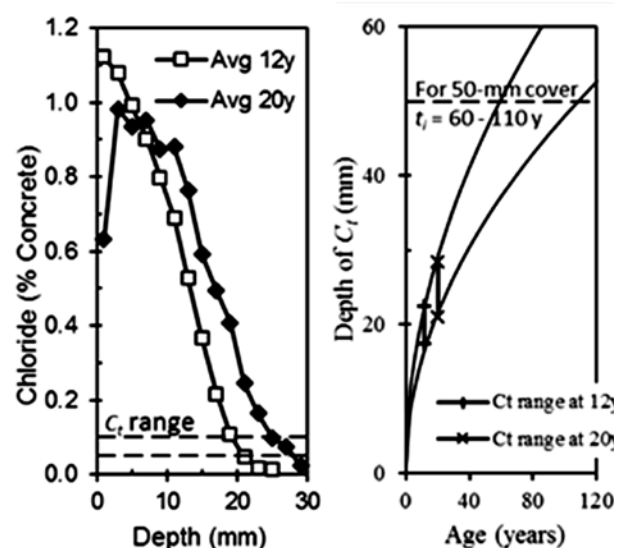
chloride levels to a depth of 45 to 50 mm. These two mixes exhibited very significant loss of material at the surface, the estimated "erosion depths" being as much as 20 to 30 mm. The surface loss is thought to be partially due to salt scaling and erosion probably exacerbated periodic high-pressure washing of the surface to facilitate visual inspection during exposure. Full discussion of this phenomenon is presented in Moffatt et al. (2017).

Treat Island Site: Hiberia Gravity-Base Structure
These blocks were placed in 1996 and sampled in 2008 and 2016 after 12 and 20 years. The chloride profiles are shown in Fig. 12 together with predictions of the future penetration of the chloride threshold using values of C_t = 0.05 and 0.10%. This was done for the purpose of estimating the residual service life. The chloride profiles are average values for 4 separate cores taken at 12 years and 3 at 20 years. For estimating the depth of penetration, x_{ct}, of the chloride threshold, C_t. The depth of penetration of the 0.05% and the 0.10% value were determined by interpolating the individual profiles (4 and 3 profiles at 12 and 20 years, respectively). For example, at 12 years the depth that C_t = 0.05% or C_t = 0.10% had penetrated ranged from 17.5 to 22.5 mm (range is 21.0 to 28.5 mm at 20 years). Figure 12 also shows curves selected to bracket the experimental data assuming the rate of penetration is proportional to root time ($x_{ct} \propto \sqrt{t}$).


Fig. 11. Chloride profiles for HVFA concrete mixes after tidal exposure periods ranging from 19 to 24 years

Fig. 12. Chloride profiles at 12 and 20 years (left) and predicting penetration of C_t (right)

The depth of penetration in the majority of HVFA concrete mixes decreased to background levels at depths between 30 to 35 mm consistent with the performance of concrete with high levels of SCM presented in Fig. 10. The exception was two HVFA mixes with LWA which showed above-background

In the case where the cover over the embedded steel is 50 mm (job specification), the data in Fig. 12 would suggest that the time to initiation is anywhere between 60 to 110 years. This is a large spread but one has to take into account the variability in the concrete performance in terms of resisting chloride penetration and the uncertainty regarding the chloride threshold required for corrosion which necessitates the use of a fairly wide range (0.05% to 0.10% in this case).

Treat Island: UHPC
Figure 13 shows ten chloride profiles for the following UHPC mixes:

- UNB-RPC: one profile at each age of 5 and 12 years
- RPC-200: one profile at each age of 13 and 20 years.
- VHSC: four profiles at 15 years and two profiles at 21 years
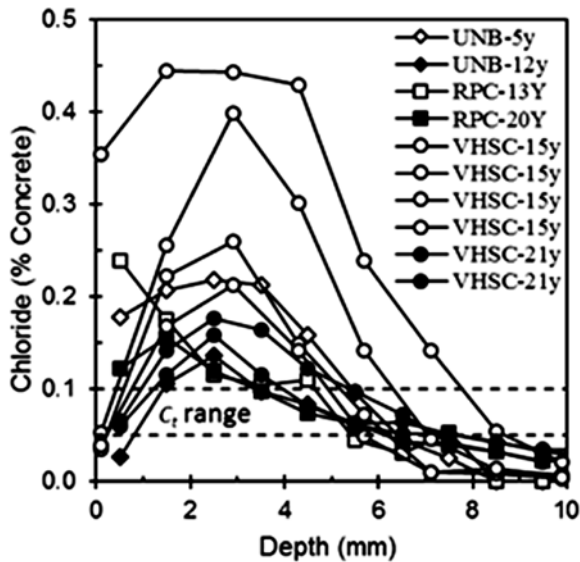
Fig. 13. Chloride profiles for various UHPC mixes after tidal exposure for periods ranging from 5 to 21 years

Initial observation, especially of the four separate 15-year-old profiles for VHSC, would suggest a high degree of variation for these data but, in comparison to all of the other profiles presented in this paper, these data occupy a fairly small band with chloride contents falling to background levels at depths ranging from 7 to 9 mm. This compares to background levels being reached at depths greater than 20 to 30 mm for the Hibernia HPC at 20 years (Fig. 12), and more than 25 to 30 mm for mixes with high levels of SCM (Figs. 10 and 11).

Close examination of the data available indicates that there is not an obvious trend of increasing chloride penetration with exposure period as was observed in all cases with the BRE data and for the SCM and HPC data from Treat Island. It is postulated by the author that, although the profiles (ignoring reductions at the surface) are consistent with concentration profiles resulting from diffusion, the curves might also represent the probability at any given depth of there being porosity that is connected to the surface. This concept is illustrated in Fig. 14. Although the porosity would not be expected to vary with depth, the volume of pores connected to the surface decreases with depth away from the surface.
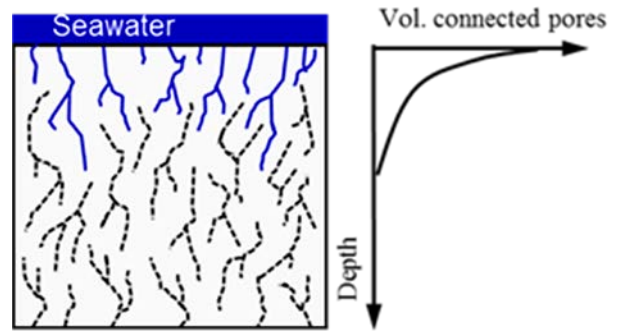
Fig. 14. Concept of reducing surface-connected porosity with depth (in figure on left: solid lines represent pores connected to the surface; broken line are pores with no direct path to the surface)

This concept was first proposed by Johansen *et al.* (1995) as a means to explain observed reductions in the diffusion coefficient, *D*, with age. They reported that, in a two-dimensional distribution of pores produced by computer simulation, the average count of surface-connected pores as a function of depth from the surface fitted "very well" to the error-function solution to Fick's 2nd-Law that is often used to calculate *D* from chloride profiles; the solution is:

$$C_{x,t} = C_0\left(x/\sqrt{4Dt}\right) \tag{1}$$

where $C_{x,t}$ is the chloride content at depth, *x*, and time, *t*, C_0 is the chloride content at the surface, and *D* is the diffusion coefficient. They hypothesized that the surface-connected porosity would quickly be inundated by chlorides and could possibly remain unchanged with time. Applying Eqn. 1 to calculate *D* from unchanging profiles at different time periods would result in *D* varying inversely proportional to *t*. It is clear from the results presented in the present study that, generally, chlorides do continue to penetrate with time except in the special case of UHPC.

Table 2 shows porosity measurements conducted on 5-year-old samples of UNB-RPC compared with cement paste sample of similar age. The paste samples are HPC (5% silica fume + 20% fly ash) and PC (100% Portland cement) both with *w/cm* = 0.40. The porosity measurements included: (i) "total porosity" calculated from the evaporable water content and (ii) "capillary porosity" determined by solvent exchange with isopropanol.

Table 2. Porosity measurements (% by volume)

	PC	HPC	UHPC
Total porosity	11.9	11.5	5.5
Capillary porosity	9.13	6.83	1.1

The total porosity includes pores of all sizes including the nano-size "gel pores" in the C-S-H. Hence, these measurements generally reflect the amount of water used during mixing and do not offer useful information on the pore structure. Isopropanol will only enter the larger pores and, thus, provides some indication of

the relative volume of the pores that are likely to contribute to mass transport (e.g. chloride ingress). The data in Table 2 show that while the total porosity of UHPC is slightly less than half that of HPC, the "capillary porosity" is more than six times lower.

If the author's supposition that the surface-connected porosity in UHPC extends to depths less than 10 mm and that chloride penetration is restricted to this depth is correct, the implications are that corrosion of steel-reinforced UHPC exposed to chlorides will not occur provided that the depth of cover is at least 10 mm. Further testing is required to test this hypothesis. A number of UHPC specimens remain in the tidal zone at Treat Island and it intended to collect these at much later ages.

4.4 Corrosion of Steel

<u>BRE Exposure Site</u>
Visible corrosion (e.g. rust staining frequently accompanied by cracking) was evident at 10 years on all of the control samples (without fly ash), regardless of strength grade. The extent of visible damage decreased with fly ash content as shown in Fig. 15 and no signs of corrosion were detected for concrete with 30% or 50% fly ash for the steel with 20 mm cover.
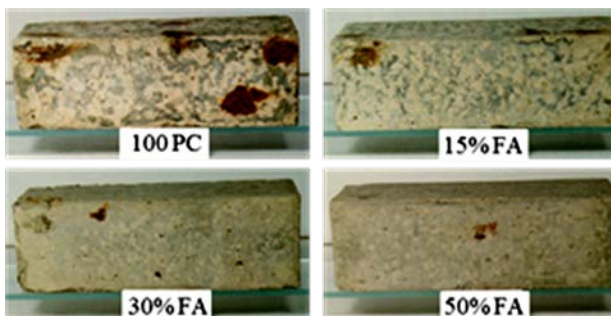
Fig. 15. Photographs of 35-MPa reinforced concrete specimens after 10 years in the BRE tidal zone

Figure 16 shows the mass loss of steel with 10-mm cover after 10 years as a function of strength grade and fly ash contents. Also shown is the mass loss of steel (10-mm cover) with time for the 35-MPa concretes. In all cases the steel with 10-mm cover exhibited some signs of corrosion after just 1 year; the signs included rust spots on bars extracted from the concrete and some measurable mass loss. Despite this early corrosion initiation, steel embedded in concrete with 30% and 50% fly ash showed very small amounts of subsequent corrosion compared with the control concrete. This is attributed to increasing fly ash levels resulting in increased electrical resistance and reduced oxygen diffusion, both of which decrease corrosion rates. Oxygen availability is limited at the mid-tide level and concrete with low oxygen diffusivity is likely to have very low corrosion rates.
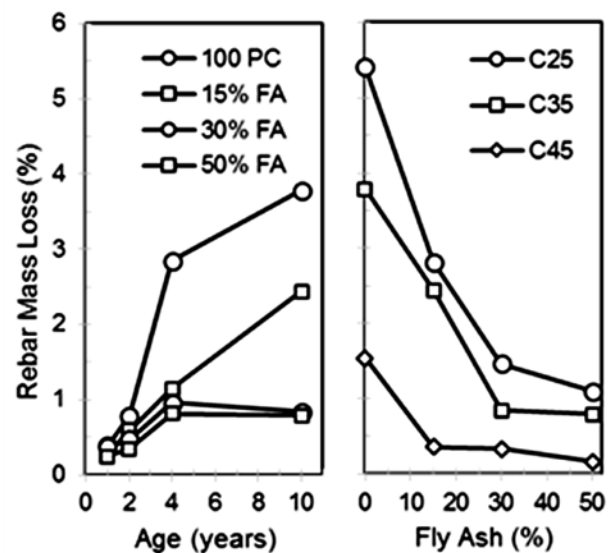
Fig. 16. Rebar mass loss as a function of time (left) and as a function of fly ash content (right). Data for rebar with 10-mm cover

<u>Treat Island Exposure Site</u>
Only a small proportion of the concrete specimens at Treat Island contain embedded steel reinforcement. Notwithstanding this statement corrosion has not been observed for any of the few reinforced concrete samples that are exposed at the mid-tide level even when chloride profiling has indicated that the chloride content at the location of the steel was many times greater than typically threshold concentrations. It is suspected that the availability of oxygen is too low to support significant corrosion propagation even if chlorides have depassified embedded steel.

As part of the CANMET study two reinforced-concrete blocks from each of four mixtures were placed in the tidal zone in 1987. The concrete with $w/cm = 0.50$ had the following binder types: (i) 100% Portland cement, (ii) 25% fly ash, (iii) 10% silica fume, and (iv) 50% slag. Reinforcing steel was placed with clear cover depths of 30, 50 and 70 mm; there was also a centrally-located steel bar with 140 mm cover. After 20 years there was no visible corrosion and, suspecting the low availability of oxygen to be the reason, one block from each mixture was relocated above the high-tide level (splash zone). After 25 years all the blocks were retrieved and subjected to electrochemical corrosion testing (half-cell and linear-polarization resistance) and chloride profiling. Data from these tests are shown in Figs. 17 and 18.

The chloride profiles (obtained on the samples that remained in the tidal zone) show the substantial benefits of SCM with regards to chloride resistance. In the control sample (100PC), chlorides had penetrated throughout the thickness of the sample with considerable chloride contents (approx. 0.2%) being detected around the centrally-mounted steel bar at a depth of 140 mm. For all of the SCM mixes the chloride concentration decreased to background levels at depths in the region of 50 to 60 mm. The

corrosion measurements (performed on the specimens that were relocated to the spray zone at 20 years) were consistent with the chloride profiles. All of the steel embedded in the PC100 concrete was in an active corrosion state and exhibited significant corrosion rates. For the concretes with SCM, only the steel with covers of 30 and 50 mm showed active corrosion and the rates of corrosion were much lower than that measured in the control sample. There was no evidence of corrosion for steel with 70 mm cover in any of the SCM concrete.
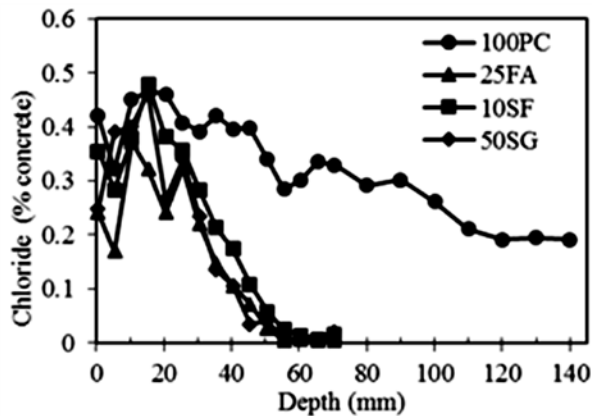

Fig. 17. Chloride profiles for reinforced-concrete specimens after 25 years in Treat Island tidal zone
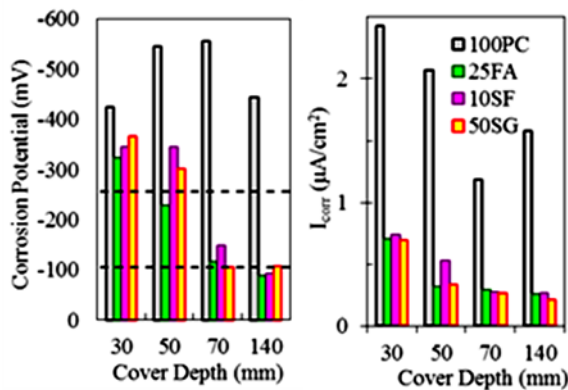

Fig. 18. Corrosion measurements for reinforced-concrete specimens after 20 years in the tidal zone and 5 years in the splash zone at Treat Island

These data are considered important as they clearly refute recent contentions that the benefits of increased resistance to chloride penetration attributed to SCM may be partially or wholly offset by SCMs lowering the chloride threshold required to initiate corrosion (Trejo and Tibbits, 2016). It has even been proposed that this could lead to a reduced service-life in concrete containing fly ash or slag in some circumstances. The data in the figures above show that this is not the case as all SCM concretes provide better protection to the steel than the concrete without SCM.

Figure 9 also supports the improved protection to steel provided by fly ash concrete. The threshold concentration, C_t, penetrates into the control concrete at a faster rate compared with the fly ash concrete. However, at very early ages, the depth of penetration of C_t is similar and, close inspection of the data would suggest that corrosion of steel with low cover (e.g. < 20-mm) might be initiated in all concretes at a similar age.

In a previous analysis of the BRE data Thomas (1996) compared rebar weight losses with the chloride concentration at the rebar to determine the lowest concentration at which corrosion losses were observed. This analysis confirmed that fly ash did reduce the threshold with values of C_t of 0.70, 0.65, 0.50 and 0.20, respectively, being determined for the concrete with 0, 15, 30 and 50% fly ash. Figure 19 shows the rate of penetration of C_t assuming the different values for concrete with varying levels of fly ash.
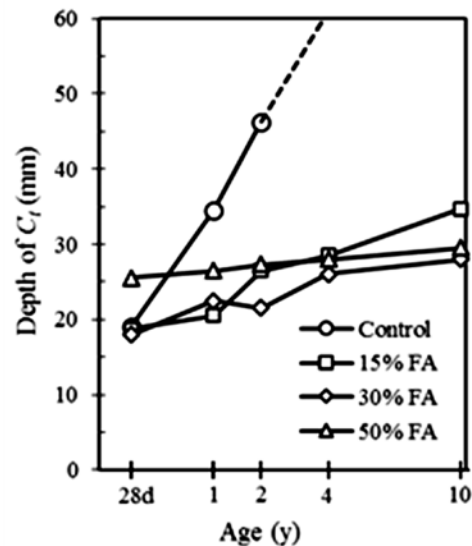

Fig. 19. Effect of fly ash on the depth of penetration of C_t (note C_t = 0.70, 0.65, 0.50 and 0.20% by mass of binder for, respectively, concrete with 0, 15, 30 and 50% fly ash)

These data do indicate that corrosion initiation may occur earlier in concrete with 50% fly ash but only if the depth of cover was less than 25 mm and conditions favoured the rapid penetration of chlorides. Provided adequate cover is ensured (for example, at least 50 to 60 mm for concrete exposed to chlorides in service), fly ash concrete is likely to provide very substantial increases in the time to corrosion.

The results of the analysis presented here demonstrate that prudence is warranted when designing laboratory tests to accelerate deterioration processes (such as using very low depths of cover to facilitate the early onset of corrosion) or such tests are unlikely to yield realistic (or useful) results.

4.5 Predicting Chloride Ingress

Numerous models have been developed to predict the service life of reinforced concrete exposed to chlorides. The author was a co-developer of the model Life-365 (Ehlen *et al.* 2009) which was later modified and incorporated in the model ConcreteWorks (Riding *et al.* 2013). This model is described briefly below and its output compared to some of the chloride profiles collected from Treat Island. Note that the BRE data are not used for this purpose as the relatively small size of the specimens eliminated one-dimensional ingress of chlorides.

Details of Life-365

Life-365 uses a finite difference implementation of Fick's second law assuming that diffusion is the sole mechanism responsible for chloride transport, which is probably a reasonable assumption for a marine tidal zone. Life-365 calculates the diffusion coefficient $D(t)$ at age t, using the following equation:

$$D(t) = D_{28} \cdot \left(\frac{28}{t}\right)^m \qquad (2)$$

where $D(t)$ = diffusion coefficient (m^2/s) at time t (days), D_{28} = early-age diffusion coefficient (m^2/s) at 28 days, and m = constant (depending on fly ash and slag content). The diffusion coefficient is corrected for temperature using the following Arrhenius relationship:

$$D(T) = D_{ref} \cdot \exp\left[\frac{U}{R} \cdot \left(\frac{1}{T_{ref}} - \frac{1}{T}\right)\right] \qquad (3)$$

where $D(T)$ = diffusion coefficient at temperature T, D_{ref} = diffusion coefficient at some reference temp. T_{ref}, U = activation energy of the diffusion process (35000 J/mol), R = gas constant and T = absolute temperature. In the model T_{ref} = 293K (20°C). The temperature T of the concrete varies with time according to the geographic location selected by the user. For a mix without SCM, the value of D_{28} is calculated from the water-to-cementing materials ratio (W/CM) using the following equation:

$$D_{28} = 1 \times 10^{(-12.06 + 2.40 W/CM)} \text{ m}^2/\text{s} \qquad (4)$$

The 28-day diffusion coefficient for silica-fume concrete, D_{SF}, is reduced based on the amount of silica fume SF (%) according Eqn 5:

$$D_{SF} = D_{PC} \cdot e^{-0.165 \cdot SF} \qquad (5)$$

where D_{PC} is the 28-day diffusion coefficient for concrete without SCM calculated according to Eqn 1. The value of m in Eqn 2 is dependent on the content of fly ash (FA) and/or slag (SG) and is determined according to Eqn 6:

$$m = 0.2 + 0.4(\%FA/50 + \%SG/70) \qquad (6)$$

The model has a built-in climate database for many locations in North America including Eastport, ME, which was used for this study. The model determines the surface concentration, C_0, based on the location,

the type of structure and the nature of exposure. For marine tidal conditions a value of C_0 = 0.8% by mass of concrete is used; this value can be changed by the user.

Comparison of Life-365 output with measured profiles
Figure 20 shows the output of Life-365 with the measured profiles at 25 years for four concrete mixes with *w/cm* = 0.40, slag content ranging from 0 to 65%, and normal density aggregate. The concrete mixes were placed in 1978 as CANMET Phase I(A); details of the concrete mix are provided in Malhotra and Bremner (1996). The only data input to Life-365 was location, tidal zone, and the w/cm and slag replacement level. The figure shows that Life-365 prediction is very close to the measured profiles for all four mixes.
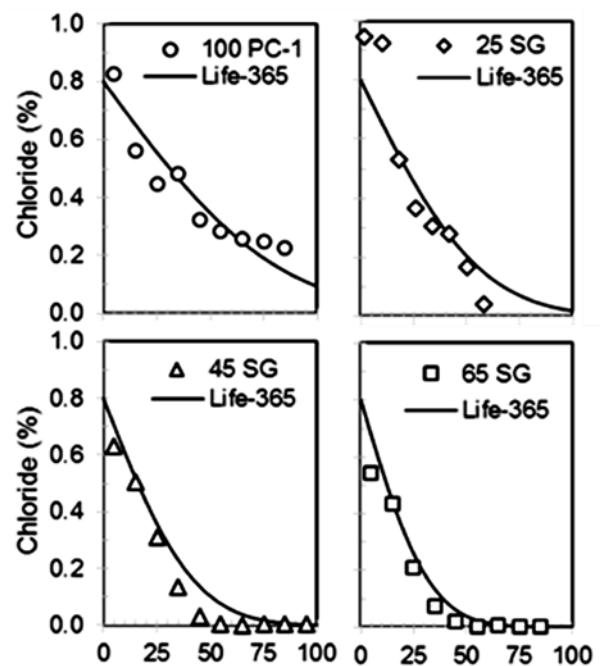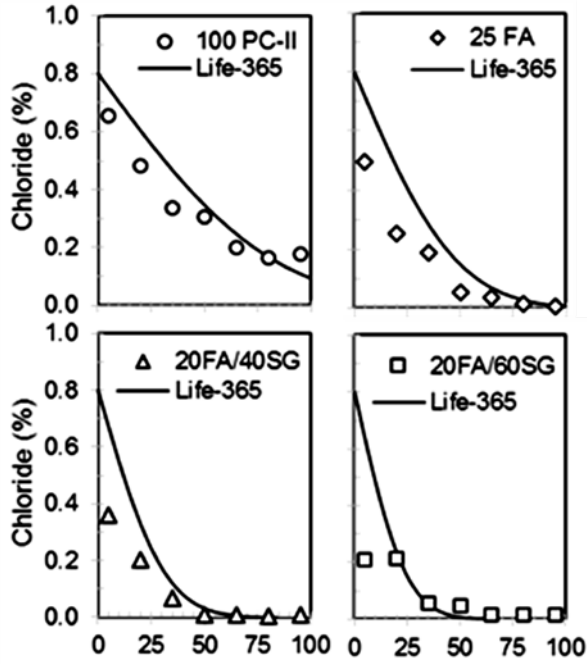

Fig. 20. Comparison of Life-365 prediction and measured chloride profile – Phase I (slag concrete, *w/cm* = 0.40, 25 years' exposure)

Life-365 was also found to closely predict the profiles measured for four very similar concrete mixes with the same *w/cm* and slag contents, but with LWA as the coarse fraction (see Thomas and Bremner, 2012); these concretes were placed in 1980 as CANMET Phase III (Malhotra and Bremner, 1996).

Figure 21 shows Life-365 predictions and measured profiles for CANMET Phase II (*w/cm* = 0.40, 100% PC, 25% fly ash and ternary blends with 20% fly ash plus 40% slag and 20% fly ash plus 60% slag). Figure 22 shows the same for Phases IV with 25% fly ash, V(A) with 80% slag, VI with 6.5% silica fume plus 13.5% fly ash, and VII with 7% silica fume. With the exception of the 7% silica fume mix (*w/cm* = 0.34) all of the concretes shown in Fig. 22 have *w/cm* = 0.40. Note that in the figure showing the chloride profile for the mix with 80% slag the Life-365 profile is for 70%

slag as this is the maximum slag replacement level allowed in the model. Also the profile for 6.5SF/13.5FA is actually for 7SF/14FA as Life-365 requires integer values for SCM levels.

Fig. 21. Comparison of Life-365 prediction and measured chloride profile – Phase II (fly ash and slag blends, *w/cm* = 0.40, 25 years' exposure)
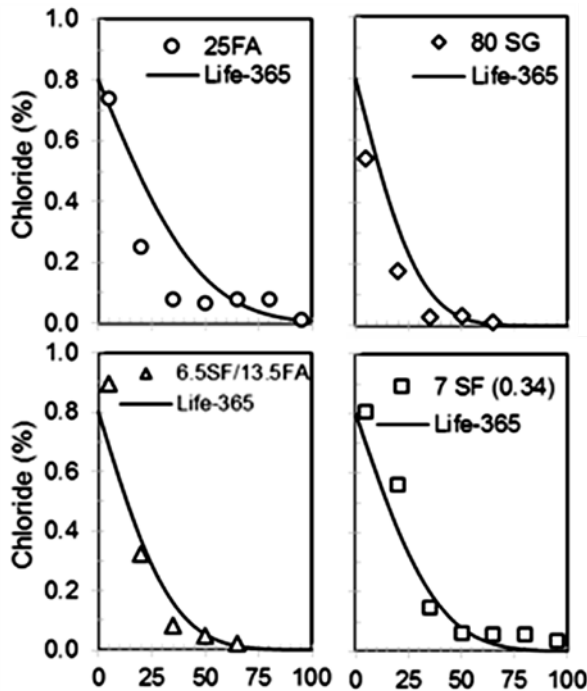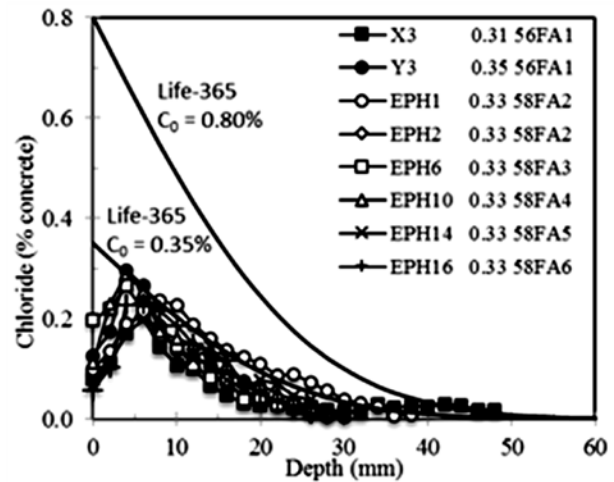

Fig. 22. Comparison of Life-365 prediction and measured chloride profile – Phase IV to VII (various SCMs, 25 years' exposure)

The fit between the model and experimental data is generally good. The one exception is the fit for 25%

fly ash (Phase IV) in Fig. 22 because of the low measured chloride contents between 25 to 50 mm.

Figure 23 shows the Life-365 profile for concrete with *w/cm* = 0.33 and 50% fly ash (highest fly ash replacement allowed in the model) compared with the measured profiles for HVFA concrete (excluding the three mixes with coarse LWA which showed high amounts of surface erosion). The default surface concentration of C_0 = 0.80% is clearly not suitable for the HVFA concrete and so the analysis was rerun with a surface concentration of C_0 = 0.35% which was found to be the closest fit considering all profiles. Even with the reduced surface concentration, the model predicts slightly greater chloride penetration than the measured values. This is partly due to the lower replacement level (50%) used in the model analysis.
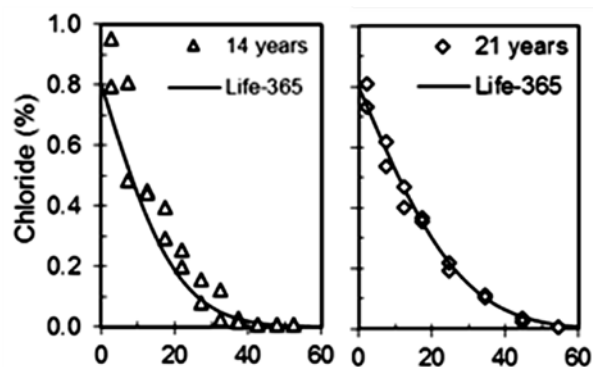

Fig. 23. Comparison of Life-365 prediction and measured chloride profile for HVFA concrete

Figure 24 compares the output from Life-365 with the 20-year-old measured profiles from the blocks produced with the concrete used for the Hibernia GBS. In this case an increase in surface concentration (to C_0 = 1.2%) was required to "match" the profiles. The high surface concentration is thought to result from the use of LWA (50% by volume of the total coarse aggregate) increasing the porosity at the surface. The model over-estimates the depth of chloride penetration (even with C_0 = 0.8%) and it is evident that the profile for these blocks is steeper than a typical chloride profile resulting from diffusion. It is possible that the lower-than-predicted penetration and the shape of the profile is a consequence of the lightweight coarse aggregate used for this concrete. The LWA was an expanded slate with a reported absorption of 6%. However, it is noteworthy that similar behaviour was not observed for the slag concretes with LWA (Phase III) which was produced from a pelletized blastfurnace slag. The differences may be attributed to the differences in the porosity and pore structure of the LWAs used and this warrants further study.
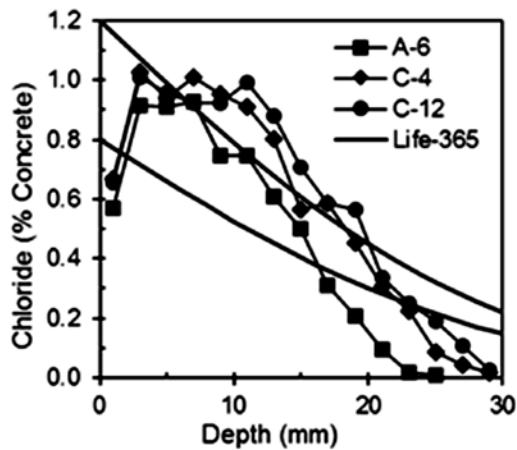
Fig. 24. Comparison of Life-365 prediction and measured chloride profile for Hibernia GBS concrete

Figure 25 shows the predicted output from Life-365 compared with chloride profiles collected for large blocks (1.5 x 1.5 x 0.5 m) exposed in the tidal zone of the Trondheim fjord in Norway (Skjølsvold *et al.* 2007). The concrete mix contains 10% silica fume and has a *w/cm* of 0.41. Climate data were used for Life-365. The predicted profiles fit the measured data extremely well.

Fig. 25. Comparison of Life-365 prediction and measured chloride profiles for silica-fume concrete in the Trondheim Fjord (Skjølsvold *et al.* 2007)

4.6   Scaling and Freeze-Thaw Damage

Only the 25-MPa control samples showed significant surface wear at the BRE site. None of these concretes were air-entrained but the freeze-thaw exposure is relatively mild and the surface loss was considered to be consistent with chemical attack.

Significant surface loss was observed for a great many of the concrete blocks at the Treat Island site. Generally, the loss was restricted to paste and mortar leaving coarse aggregates exposed. The extent of loss was visibly more noticeable on mixes with higher SCM replacement levels, especially for concrete with *w/cm* = 0.50 and 0.60. Most concrete with *w/cm* $\leq$ 0.40 showed little surface scaling with the exception of the HVFA mixes all of which exhibited some mass loss at the surface.

The blocks were cleaned thoroughly with a high-pressure water spray approximately every two years to facilitate visual inspection. It is not know to what extent the high-pressure spraying contributed to the observed surface loss. Notwithstanding the precise cause(s) of the surface loss – whether pressure washing or salt scaling, or a combination – it is clear that the concrete with high levels of SCM with moderate to high *w/cm* (0.50 to 0.60) are more susceptible.

Although the data shown above show no evidence of seawater exacerbating ASR, observations made during other studies at Treat Island do indicate that ASR can render air-entrained concrete susceptible to freeze-thaw attack. Figure 26 shows photographs of concrete specimens that show varying levels of ASR expansion. It is apparent that damaging freeze-thaw attack starts to occur when some threshold level of ASR expansion has occurred. Specimens that expand up to 0.15% or so remain intact and do not seem to undergo any freeze-thaw-related damage. Once concrete expands by more than approximately 0.2% due to ASR, freeze-thaw deterioration seems to take over leading to significant spalling of the concrete. It is suggested that the "threshold level of expansion" coincides with the establishment of a continuous crack system in the concrete.
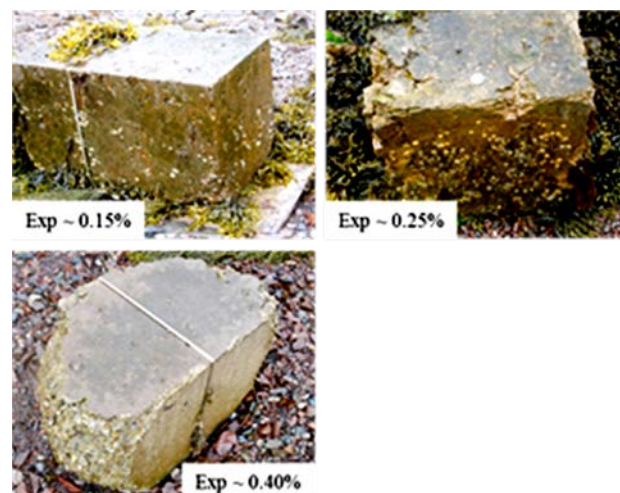

Fig. 26. Freeze-thaw damage in ASR-affected concrete at Treat Island

4.7   Performance Indicators

Early-age performance data, such as electrical resistivity or conductivity, are not available for the concrete mixes placed at either exposure site. However, electrical conductivity measurements (ASTM C 1202) were performed on cores taken from blocks that were retrieved from Treat Island after various periods of exposure. Figure 27 shows the results of the C 1202 test, commonly referred to as the "rapid chloride permeability test" or RCPT, plotted against the depth of chloride penetration. For this analysis the depth, $X_{0.1}$, at which the chloride content is equal to, $C_x = 0.1\%$, is used to represent the depth

of chloride penetration. This value was chosen in preference to 0.05% as this value is too close to the background chloride levels for some of the concretes.

There is a reasonably good relationship between these two parameters. Of course, what is required is a test that is conducted on the concrete at early age. It is suggested that such a test could also be based on electrical measurements with corrections made for the pore-solution conductivity/resistivity and, if feasible, the binding capacity of the binder. Accelerated curing at elevated temperature is required to determine the long-term performance of different binders. Studies of this nature are currently ongoing at UNB and the marine data presented here will be critical for benchmarking these tests.
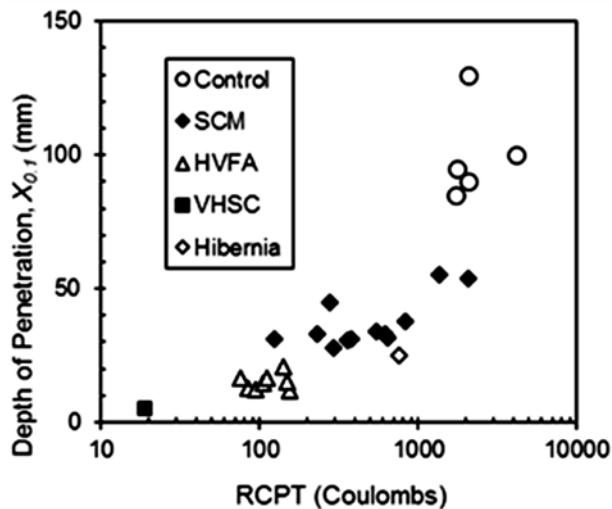
Fig. 27. Relationship between electrical charge passed in RCPT and the depth of chloride penetration

The development of suitable performance testing is essential if codes are to move away from the prescriptive-type of specification that relies on minimum cement content, maximum *w/cm* and, perhaps, binder type. Only performance testing can really allow all of the possible alternatives for achieving adequate durability in a marine environment to be considered.

5.0   SUMMARY

The data presented from the two marine exposure sites clearly emphasize the importance of SCMs for producing concrete with a high-resistance to chloride-ion penetration. Much of the benefits may not be realized by short-term laboratory tests that fail to take account of the pore-structure refinements that take place over many years for some of the more slowly-reacting SCMs. However, some caution may be warranted when using relatively high SCM replacements in concrete exposed to multiple cycles of freezing and thawing.

References

Alexander, M.G., Nganga, G. 2016. Introduction: importance of marine concrete structures and durability design. In Marine Concrete Structures: Design, Durability and Performance (M.G. Alexander, Editor), Woodhead Publishing, Duxford, U.K., pp. 1-13.

Angst, U., Elsener, B., Larsen, C.K., Vennesland, Ø. 2009. Critical chloride content in reinforced concrete – A review. Cement and Concrete Research, 39; 1122-1138.

De Weerdt, K., Orsáková, D., Müller, A., Larsen, K., Pedersen, B., Geiker, M. 2016. Towards the understanding of chloride profiles in marine exposed concrete, impact of leaching and moisture content. Construction and Building Materials, 120: 418–431.

Ehlen, M.A., Thomas, M.D.A. and Bentz, E.C. 2009. Life-365 Service Life Prediction Model™ Version 2.0. Concrete International, May, pp. 41-46.

Folliard, K.J., Thomas, M.D.A., Fournier, B., 2008. The Effects of Potassium Acetate De-icing Chemicals on the Performance of Concrete Containing Fly Ash: A Literature Review. EPRI, Palo Alto, CA, 1018167.

Fournier, B., Chevrier, R., Bilodeau, A., Nkinamubanzi, P-C., Bouzoubaa, N. 2016. Comparative field and laboratory investigations on the use of supplementary cementing materials (SCMs) to control alkali-silica reaction (ASR) in concrete. Proc. 15th Int. Conf. on Alkali Aggregate Reaction in Concrete. Sao Paulo, Brazil, Paper 271.

Gjørv, O., Vennesland, Ø. 1979. Diffusion of chloride ions from seawater into concrete. Cement and Concrete Research, 9: pp. 229-238.

Johannesson, B., Yamada, K., Nilsson, L-O., Hosokawa, Y. 2007. Multi-species ionic diffusion in concrete with account to interaction between ions in the pore solution and the cement hydrates. Materials and Structures, 40: 651–665.

Johansen, V., Goltermann, P., Thaulow, N. 1995. Chloride transport in concrete. Concrete International, 17(70): 43-44.

Malhotra, V.M., Bremner, T. 1996. Performance of Concrete at Treat Island, USA: CANMET Investigations, In Performance of Concrete in Marine Environment, Third CANMET/ACI International Conference SP-163, pp. 1-52.

Mehta, P.K. 1980. Durability of Concrete in Marine Environment--A Review. In Performance of Concrete in Marine Environment, ed. V.M. Malhotra. ACI Publication SP-65, pp. 1-20.

Moffatt, E.G., Thomas, M.D.A., Fahim, A. 2017. Performance of high-volume fly ash concrete in marine environment. Cem. Concr. Res., 102: 127-135.

Nishibayashi, S., Okada, K., Kawamura, M., Kobayashi, K., Kojima, T., Miyagawa, T., Nakano,K., Ono, K.1992. "Alkali-silica reaction - Japanese experience." The Alkali-Silica Reaction in Concrete. Blackie and Sons Ltd., Glasgow.

Riding, K., Thomas, M.D.A. and Folliard, K.J. 2013. "Apparent Diffusivity Model for Concrete Containing Supplementary Cementitious Materials." ACI Materials Journal, 110 (6): 705-714.

Santhanam, M., Otieno, M. 2016. Deterioration of concrete in the marine environment. In Marine Concrete Structures: Design, Durability and Performance (M.G. Alexander, Editor), Woodhead Publishing, Duxford, U.K., pp. 137149.

Skjølsvold, O., Justnes, H., Hammer, T., Fidjestøl, P. 2007. Long-term chloride intrusion in field-exposed concrete with and without silica fume, Proc. 9th CANMET/ACI Conference on Fly Ash, Silica Fume, Slag and Natural Pozzolans in Concrete, ACI SP-242, American Concrete Institute, Detroit: 199–210.

Thomas, M.D.A., 1991. Marine performance of pfa concrete. Mag Concrete Res;43(156):71–185.

Thomas, M.D.A., Bamforth, P.B. 1999. Modelling chloride diffusion in concrete: effect of fly ash and slag. Cem. Conc. Res., 29: 487-495.

Thomas, M.D.A., Bremner, T, 2012. Performance of lightweight aggregate concrete containing slag after 25 years in a harsh marine environment. Cement and Concrete Research, 42: 358–364

Thomas, M.D.A., Matthews, J.D. 1996. Chloride penetration and reinforcement corrosion in marine-exposed fly ash concretes. 3rd CANMET/ACI Int. Conf. on Concrete in a Marine Environment (Malhotra VM, editor), ACI SP-164, American Concrete Institute, 317–38.

Thomas, M.D.A. and Matthews, J.D. 2004. Performance of PFA concrete in a marine environment – 10 year results. Cem. Conc. Comp., 26(1): 5-20.

Thomas, M.D.A., Green, B., O'Neal, E., Perry, V., Hayman, S., Hossack, A. 2012. Marine Performance of UHPC at Treat Island. In Proc. 3rd Int. Symp. on UHPC and Nanotechnology for High Performance Construction Materials (Editors Michael Schmidt et al.), Kassel, pp. 365-370.

Trejo, D. and Tibbits, C. 2016. "The Influence of SCM Type and Quantity on the Critical Chloride Threshold," ACI SP-308—Chloride Thresholds and Limits for New Construction: 1-20.